Laser-Induced Fluorescence Spectra, Structure, and the Ring-Twisting and Ring-Bending Vibrations of 1,4-Benzodioxan in Its S_0 and $S_1(\pi,\pi^*)$ States

Juan Yang, Martin Wagner, and Jaan Laane*

Department of Chemistry, Texas A&M University, College Station, Texas 77843-3255

Received: April 21, 2006; In Final Form: June 16, 2006

The laser-induced fluorescence (LIF) spectra, both the fluorescence excitation spectra (FES) and single vibrational level fluorescence spectra (SVLF) from several different vibronic states, along with the ultraviolet (UV) absorption spectra of 1,4-benzodioxan have been recorded and analyzed. A detailed energy map has been constructed for four low-frequency vibrations and their combinations for both the S_0 and $S_1(\pi,\pi^*)$ electronic states. These are ν_{48} (ring-bending), ν_{25} (ring-twisting), ν_{47} (ring-flapping), and ν_{24} (skeletal-twisting). Both the experimental and ab initio calculations show the molecule to be twisted in both the S_0 and $S_1(\pi,\pi^*)$ states with high barriers to planarity. The experimentally determined ring-twisting quantum states, which are confined to the lower regions of the potential energy surface, were used to calculate one-dimensional potential functions in terms of the twisting coordinates, and the extrapolated barriers were estimated to be 5700 and 4200 cm^{-1} for the S_0 and S_1 states, respectively. Two-dimensional calculations, which included the interactions with the bending modes, gave values of 3906 and 1744 cm^{-1}, respectively. The S_0 value compares favorably with the ab initio value of 4095 cm^{-1}.

Introduction

In recent years, we have been studying the structures and conformations of bicyclic aromatic compounds utilizing the laser-induced fluorescence spectroscopy of jet-cooled molecules[1−8] along with ultraviolet absorption spectra. Recent work has been published on molecules in the indan family[3−6] and 1,2-dihydronaphthalene.[8] In the present paper, we present our results on 1,4-benzodioxan (14BZD), which is related to the simpler molecule 2,3-dihydro-1,4-dioxin (DHD). We have already reported the ground-state vibrational frequencies (infrared and Raman) along with density functional theory (DFT) computations for this molecule as well as the related molecule tetralin (TET).[9] In our work here, we concentrate on the ring-twisting and ring-bending vibrational modes of 14BZD and utilize these to analyze the characteristics of the potential energy surfaces (PESs) for the conformational changes of this molecule in its S_0 ground and $S_1(\pi,\pi^*)$ electronic excited states. These PESs allow us to understand how electronic transitions affect the structures and forces of molecules, and, hence, some of the important contributions to photochemical reactions.

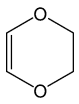

DHD

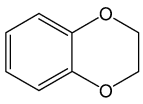

14BZD

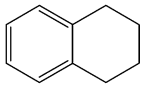

TET

Experimental Section

The sample of 1,4-benzodioxan (97% purity) was purchased from Aldrich Chemical Co. and further purified by vacuum distillation.

Ultraviolet absorption spectra were recorded on a Bomem DA8.02 Fourier transform spectrometer using a deuterium lamp source, a quartz beam splitter, and a silicon detector in the 20 000−50 000 cm^{-1} region. The vapor-phase sample was contained in a 20 cm glass cell with quartz windows. Ultraviolet absorption spectra were collected at ambient temperatures, and the vapor pressure within the cell was about 200 mTorr. Resolutions of 0.25 and 0.5 cm^{-1} were used, and more than 10 000 scans were averaged.

The FES and SVLF spectra were recorded using a Continuum Powerlite 9020 Nd:YAG laser that pumped a Continuum Sunlite OPO and FX-1 ultraviolet extension unit. FES spectra were obtained at 0.5 cm^{-1} resolution, and SVLF spectra were taken with a spectral resolution of 1 cm^{-1}. Both spectra were recorded under jet-cooled conditions. More details are provided elsewhere.[1−8]

Calculations

Theoretical calculations were carried out using the GAUSSIAN 03 package.[10] The calculations for the structure and vibrational frequencies for the S_0 ground state have been reported previously.[9] Preliminary calculations for the structural parameters and vibrational frequencies for the $S_1(\pi,\pi^*)$ excited state have been carried out and can be found elsewhere.[11] Table 1 lists the calculated energies for the planar (C_{2v}) and bent (C_s) structures of 14BZD in its S_0 state relative to the energy minima at twisted (C_2) conformations.

The twisting angle τ and the bending angle θ are as defined in Figure 1. By fixing the dihedral angle D(−O−C−C−O−), the twisting angle τ is confined to be a constant during the structural optimization. The energies for different conformations with different twisting angles were computed from the MP2/6-31G(d) calculations. A one-dimensional calculated potential energy curve for the 14BZD S_0 state with respect to the twisting coordinate τ is presented in Figure 2. For this basis set the calculated barrier is 4431 cm^{-1}. Similarly, by fixing the dihedral angle D(−C═C−O−C−), the bending angle θ can also be fixed during the optimization. The corresponding relative energies and the one-dimensional potential energy curve in the S_0 state with respect to the bending coordinate θ are presented in Figure 3.

10.1021/jp062474b CCC: $33.50
Published on Web 07/22/2006

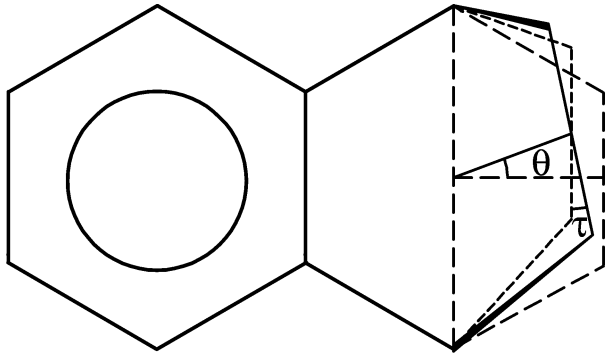

Figure 1. Definition of ring-twisting coordinate τ and the ring-bending coordinate θ for 1,4-benzodioxan and related molecules.

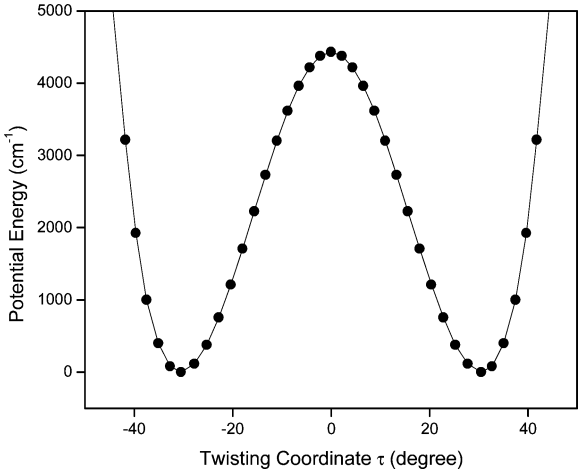

Figure 2. One-dimensional ring-twisting potential energy from MP2/6-31G(d) calculations for 1,4-benzodioxan.

TABLE 1: Calculated Relative Energies (cm^{-1}) for Different Structures of 1,4-Benzodioxan in Its S_0 Ground State

	HF	B3LYP	MP2		
structure	6-311++G (d,p)	6-311++G (d,p)	6-31G (d)	6-311++G (d,p)	cc-pVTZ
C_{2v} (planar)	3572	3265	4431	4509	4095
C_s (bent)	2219	2360	2890	2576	2722
C_2 (twisted)	0	0	0	0	0

All energies are relative to the energy minima at the twist conformations.

If both τ and θ are fixed at the same time, then the relative energies for conformations with specific twisting and bending coordinates can be calculated. By varying the fixed τ and θ values, a two-dimensional potential energy surface that consists of hundreds of data points can be generated, as shown in Figure 4.

Vibrational Hamiltonian

For molecules that have two strongly coupled large-amplitude vibrations, as is the case for 14BZD with its ring-twisting ν_{25} and the ring-bending ν_{48} vibrations, the two-dimensional vibrational Hamiltonian operator is given by

$$\hat{\mathbf{H}}_{\text{vib}} = -\frac{\hbar^2}{2}\left[\frac{\partial}{\partial\tau} g_{44}(q_4, q_5)\frac{\partial}{\partial\tau} + \frac{\partial}{\partial\tau} g_{45}(q_4, q_5)\frac{\partial}{\partial\theta} + \frac{\partial}{\partial\theta} g_{45}(q_4, q_5)\frac{\partial}{\partial\tau} + \frac{\partial}{\partial\theta} g_{55}(q_4, q_5)\frac{\partial}{\partial\theta}\right] + \hat{\mathbf{V}}(\tau, \theta) \quad (1)$$

where τ and θ are the ring-twisting and ring-bending coordinates, respectively. The g_{44} and g_{55} expressions are the reciprocal reduced masses for the ring-twisting and ring-bending vibrations, respectively. The g_{45} term is the interaction cross term for these two vibrations. The methodology and vectors for these calculations are published elsewhere.[12]

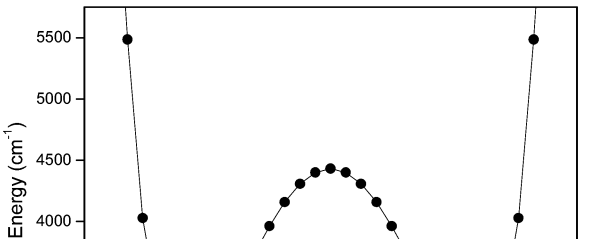

Figure 3. One-dimensional ring-bending potential energy curve from MP2/6-31G(d) calculations for 1,4-benzodioxan. The energy is relative to the twisting minima.

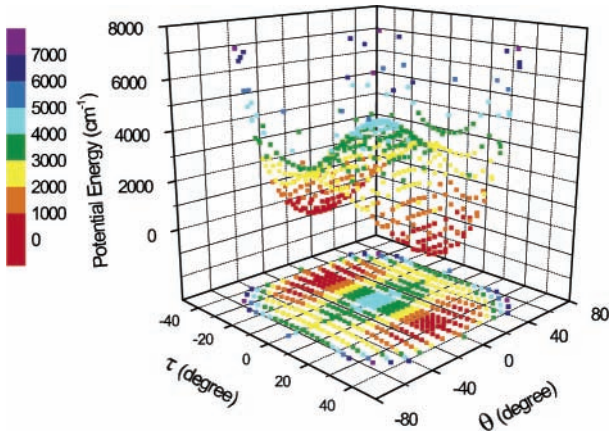

Figure 4. Two-dimensional potential energy for 1,4-benzodioxan S_0 state from MP2/6-31G(d) calculations.

Assignment of Spectra

14BZD is related to 2,3-dihydro-1,4-dioxin (DHD), which we have studied previously.[13] In 14BZD, a planar benzene ring replaces the double bond, but this molecule is also expected to have twisted C_2 symmetry with a high barrier to planarity. The MP2/cc-pVTZ calculation predicts the molecule to have a barrier to planarity of 4095 cm^{-1} in the S_0 state. With such a high barrier, the energy levels close to the bottoms of the twisting potential energy wells are nearly degenerate. The symmetry species of the nearly degenerate ground states ($\nu_T = 0,1$) are A_1 and A_2, respectively, assuming the molecule has perturbed C_{2v} symmetry.

Figures 5 and 6 show the jet-cooled fluorescence excitation spectrum (FES) and the room-temperature ultraviolet (UV) absorption spectrum of 14BZD in the 0−900 cm^{-1} and 900−1800 cm^{-1} regions, respectively, relative to the electronic band origin 0_0^0 at 35 563.1 cm^{-1}. Figure 7 shows the FES spectrum under relatively hot conditions compared with the UV absorption spectrum. This was achieved by decreasing the backing pressure of the He carrier gas and by increasing the distance from the nozzle to the laser beam. Table 2 presents the frequencies and

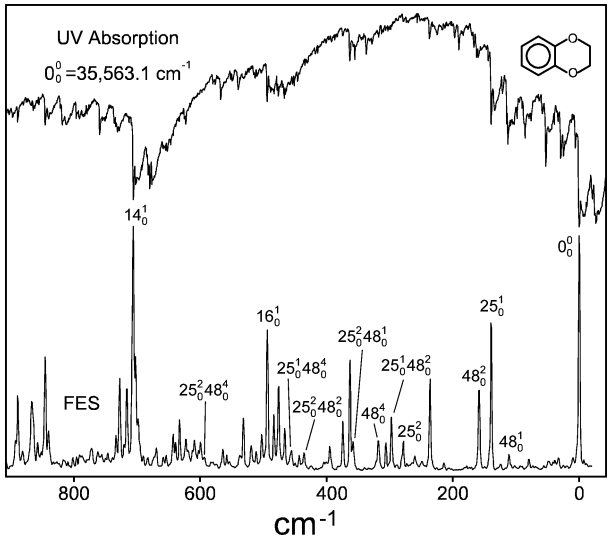

Figure 5. Fluorescence excitation spectra of jet-cooled 1,4-benzodioxan and ultraviolet absorption spectra at ambient temperature in the 0−900 cm^{-1} region. The band origin 0_0^0 is at 35 563.1 cm^{-1}.

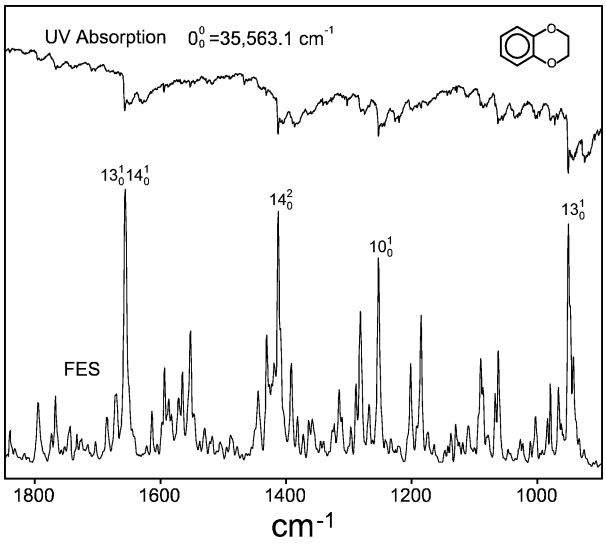

Figure 6. Fluorescence excitation spectra of jet-cooled 1,4-benzodioxan and ultraviolet absorption spectra at ambient temperature in the 900−1800 cm^{-1} region.

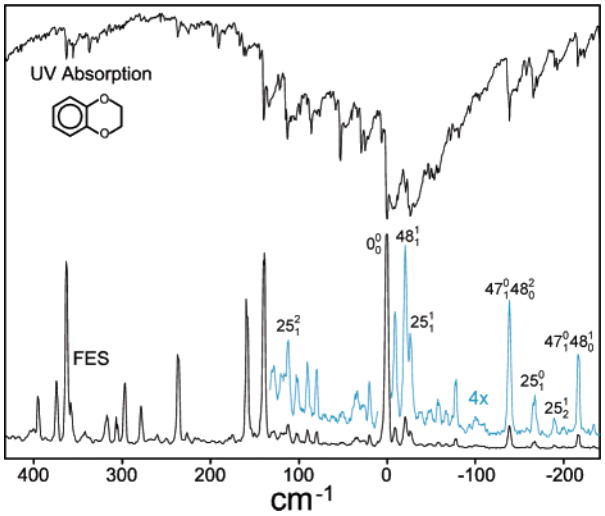

Figure 7. Ultraviolet absorption spectra and fluorescence excitation spectra of hot bands of 1,4-benzodioxan.

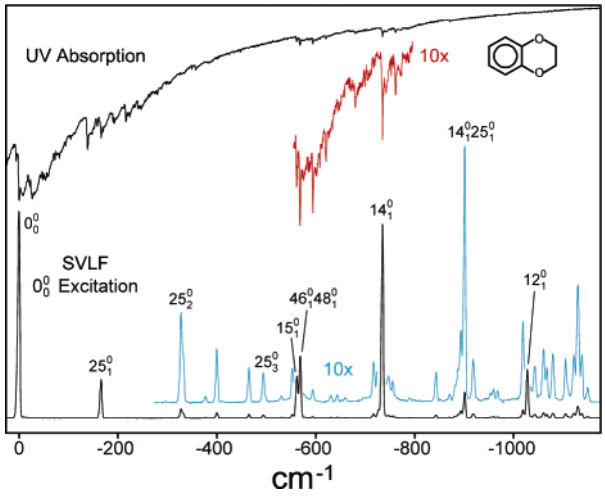

Figure 8. Single vibronic level fluorescence spectra of jet-cooled 1,4-benzodioxan with excitation of the 0_0^0 band at 35 563.1 cm^{-1} and the ultraviolet absorption spectra at ambient temperature.

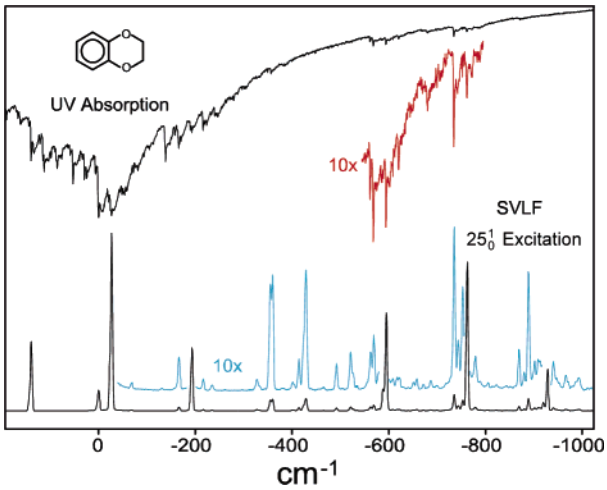

Figure 9. Single vibronic level fluorescence spectra of jet-cooled 1,4-benzodioxan with excitation of the 25_0^1 band (0_0^0 + 139.6 cm^{-1}) and the corresponding ultraviolet absorption spectra at ambient temperature.

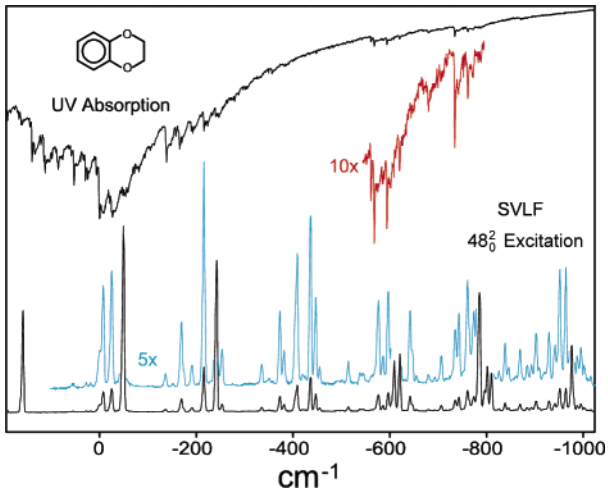

Figure 10. Single vibronic level fluorescence spectra of jet-cooled 1,4-benzodioxan with excitation of the 48_0^2 band (0_0^0 + 159.3 cm^{-1}) and the ultraviolet absorption spectra at ambient temperature.

TABLE 2: Fluorescence Excitation Spectra (FES), Ultraviolet (UV) Absorption Frequencies (cm^{-1}), and Assignments for 1,4-Benzodioxan[a]

this work						GH[b]				
FES		UV		inferred[c]	assignment	FES		UV		assignment
		−761.8	w	−761.2	$14_1^0 25_1^1$					
		−734.7	m	−734.7	14_1^0					
		−620.5	w	−620.6	$25_1^1 27_2^0$					
		−594.1	m	−594.1	27_2^0					
		−568.4	m	−568.4	15_1^0					
		−561.5	w	−561.5	$46_1^0 48_1^0$					
		−356.6	w	−356.9	27_2^1					
		−246.7	m		?					
		−240.8	m	−241.6	25_4^3			−240.88	vw	$24_2^2 48_1^1$
		−233.7	m	−234.2	$25_1^1 48_2^0$					
		−217.2	w	−217.3	$47_1^0 48_0^1$					
−217	w	−216.0	s	−216.0	25_3^2			−216.10	w	24_2^2
		−192.7	s	−192.1	25_2^1			−193.13	vw	25_2^1
−190	vw	−190.1	m	−190.1	$25_1^0 48_1^1$			−189.98	vw	$25_1^0 48_1^1$
		−170.0	w	−171.0	$25_2^0 48_0^2$					
		−167.3	m		?			−167.87	w	$47_1^0 48_0^1$
−166	vw	−165.6	s	−165.6	25_1^0			−166.06	w	25_1^0
−138	w	−138.4	vs	−137.8	$47_1^0 48_0^2$	−138	vvw	−138.92	m	24_1^1
		−104.6	w	−104.3	48_1^0					
		−93.6	m	−93.1/−94.1	$25_2^0 47_0^2/48_4^4$			−94.33	vvw	48_4^4
		−85.6	w	−85.8	$25_1^0 48_0^1$			−86.08	vvw	
		−81.4	m		?			−81.88	m	25_3^3
−78	vw			−78.2	25_3^3			−77.19	m	$25_2^2 48_1^1$
		−71.9	m	−73.0/71.6	$47_0^2 48_3^0/48_3^3$			−71.67	m	48_3^3
		−67.4	w	−68.1	$25_0^1 48_2^0$			−68.16	w	$47_0^1 48_4^3$
		−59.0	m	−59.9	47_1^2					
		−52.3	m	−52.0	25_2^2			−53.81	m	25_2^2
		−48.3	w	−48.4	48_2^2			−48.53	m	48_2^2
		−31.1	vs	−28.8	14_1^1					
−26	w	−26.5	vvs	−26.0	25_1^1	−26	vw	−26.91	s	25_1^1
		−24.5	vs	−24.5	48_1^1			−24.66	s	48_1^1
−21	w	−21.0	m		?			−21.57	m	$25_1^1 47_0^1 48_1^0$
		−12.0	w	−12.0	24_1^1					
		−6.3	vs	−6.3	$25_1^0 48_0^2$					
0	vs	0.0	vvs	0.0	0_0^0	0	vs	0	vs	0_0^0
		6.2	m		?			6.03	s	$47_0^1 48_1^0$
		24.7	s		?			24.40	m	$25_1^1 47_0^3 48_3^0$
		29.1	s	30.9/29.5	$48_2^3/47_0^2 48_2^0$			28.89	s	$47_0^2 48_2^0$
		52.9	vs	52.9/55.0	$25_1^1 48_0^1/48_1^2$			52.61	s	$47_0^3 48_3^0$
						54	vvw	54.13	vw	24_0^1
		58.4	m	58.7	25_3^4					
80	w	79.5	vw	79.8	48_0^1					
		85.8	s	85.8	25_2^3			85.31	m	25_2^3
111	w	112.8	vs	112.7	25_1^2	114	vw	112.39	m	25_1^2
		133.6	s	133.3	$25_1^1 48_0^2$			133.38	vw	
139	s	139.6	vs	139.6	25_0^1	139	s	139.30	s	25_0^1
159	s	159.3	w	159.3	48_0^2	159	vw	159.39	w	48_0^2
		166.9	m	168.7	$16_1^1 25_0^1$			166.50	w	$25_0^1 47_0^2 48_2^0$
		190.6	m		?			190.43	w	$25_0^1 47_0^3 48_3^0$
236.5	s	237.2	m	237.2/238.6	$47_0^2/48_0^3$	237	vw	236.72	w	47_0^2
278	m	278.3	w	278.3	25_0^2	278	vvw	278.36	vw	25_0^2
297	m			298.9	$25_0^1 48_0^2$					
306	m			306.5	24_0^1					
318	m	317.8	w	317.0/317.8	$47_0^2 48_0^1/48_0^4$					
		337.1	m	336.6	$23_0^1 25_1^1$					
		355.4	w	356.8	$23_0^1 25_1^0 48_0^2$					
358	m	357.8	vw	358.1	$25_0^2 48_0^1$					
363	s	363.1	m	363.1	23_0^1	363	w	362.88	m	23_0^1
374	m	374.3	w	376.8	$25_0^1 47_0^2$	374	vvw	374.39	vw	$25_0^1 47_0^2$
395	m			396.5	$47_0^2 48_0^2$					
435	w	434.2	vw	437.6	$25_0^2 48_0^2$					
443	w	442.8	vw	446.2	$24_0^1 25_0^1$					
455	w			457.4	$25_0^1 48_0^4$					
465	m	465.1	vw	465.8	$24_0^1 48_0^2$					
		467.2	w	467.0	$16_0^1 25_1^1$					
		470.0	vw	469.0	$16_0^1 48_1^1$					
476	s	476.2	w	474.4/475.9	$47_0^4/48_0^6$					
483	m	483.1	w	483.1	39_0^1					

TABLE 2 (Continued)

this work						GH[b]			this work						GH[b]		
FES		UV		inferred[c]	assignment	FES	UV	assignment	FES		UV		inferred[c]	assignment	FES	UV	assignment
493	s	493.5	m	493.5	16_0^1				1404	m	1404.3	m	1404	21_0^2			
502	m	503.3	vw	502.7	$23_0^1 25_0^1$				1409	s	1408.6	m	1408	$14_0^1 21_0^1$			
511	w	510.3	vw	515.5	$25_0^2 47_0^2$				1413	vs	1412.8	s	1412	14_0^2		1410 s	18_0^2
		513.3	w	513.2	$14_0^1 25_2^1$				1419	m	1419.7	vw		?			
519	m			522.4	$23_0^1 48_0^2$				1431	s	1431.6	m		?			
531.5	m	531.1	vw	531.1	15_0^1				1444	m	1444.2	w		?			
		539.5	m	540.3	$14_0^1 25_1^0$				1552	s	1552.5	m	1553	$14_0^2 25_0^1$			
553	vw	552.0	vw	553.0	25_0^4				1565	m	1565.1	vw	1567	$14_0^1 21_0^1 48_0^2$			
557	w			555.0	$47_0^2 48_0^4$				1571	m			1572	$14_0^2 48_0^2$			
564	w	563.6	vw	562.9	$39_0^1 48_0^1$				1594	s	1594.2	m	1594	$14_0^1 37_0^1$			
		567.4	m	567.5	$14_0^1 47_1^0 48_0^2$				1613	m	1614.2	vw		?			
599	w			600.3	$23_0^1 47_0^2$						1629.1	m	1630	$13_0^1 14_0^1 25_1^1$			
609	m			612	24_0^2				1650	m	1649.5	m	1650	$20_0^1 21_0^1$		1642 s	$14_0^1 18_0^1$
622	m	622.8	m	622.7	$25_0^1 39_0^1$				1656	vs	1656.5	s	1657	$13_0^1 14_0^1$			
632	m	633.1	w	633.1	$16_0^1 25_0^1$				1671	m			1672	$14_0^1 39_0^2$			
639	m	638.8	vw	641.4	$23_0^1 25_0^2$				1685	m	1685.3	w	1686	$14_0^1 21_0^1 25_0^2$			
642.5	m	643.0	vw	642.7	$39_0^1 48_0^2$				1767	m	1766.6	m	1769	$14_0^1 15_0^2$			
653	w	652.2	m	655.1	$16_0^1 48_0^2$				1794	m	1795.2	m	1797	$13_0^1 14_0^1 25_0^1$			
658	w	657.3	vw	658.6	$23_0^1 25_0^1 48_0^2$				1839	m	1839.7	w		?			
669	m			670.7	$15_0^1 25_0^1$				1897	m	1897.1	m	1902	13_0^2			
		676.6	s	677.1	14_1^2						1930.9	m		?			
		679.6	vs	679.4	$14_0^1 25_1^1$	678	vs	$18_0^1 25_1^1$	1957	s	1958.0	m	1959	$10_0^1 14_0^1$			
		682.3	s	681.4	$14_0^1 48_1^1$				1987	m	1986.8	m		?			
690	w			690.7	$15_0^1 48_0^2$				2013	m				?			
		696.8	m		?				2202	m	2202.0	m	2204	$10_0^1 13_0^1$			
698	m			702.3	$24_0^1 47_0^2 48_0^2$				2363	m	2363.1	m	2364	$13_0^1 14_0^2$			
702	s	702.0	s	702.0	21_0^1												
706	vs	705.9	vs	705.9	14_0^1	704	vs	18_0^1									
716	m				?												
727	m	728.0	m	726.2	23_0^2												
		731.1	m	730.6	?												
		735.9	m	735.0	$14_0^1 47_0^2 48_2^0$												
		758.8	m	758.8	$14_0^1 25_1^1 48_0^1$												
		791.3	m	791.7	$14_0^1 25_2^3$												
		812.3	m	812.9	$13_0^1 47_1^0 48_0^2$												
		818.5	m	818.7	$14_0^1 25_1^2$												
840	m	840.2	m	839.5	$21_0^1 25_0^1$												
845	s	845.3	m	845.5	$14_0^1 25_0^1$	842	w	$21_0^1 25_0^1$									
857	m	857.8	w	856.6	$16_0^1 23_0^1$												
864	m	864.3	w	865.5	$14_0^1 48_0^2$												
867	m	867.5	w	867.6	$23_0^2 25_0^1$												
888	m	888.9	m	888.9	37_0^1												
		920.9	m	920.2	$13_0^1 14_1^1$												
		924.9	s	924.8	$13_0^1 25_1^1$	924	s	$14_0^1 25_1^1$									
938	m	939.5	w	939.2	$21_0^1 47_0^2$												
943	s	943.0	m	943.1	$14_0^1 47_0^2$												
948	s	947.1	m	947.1	20_0^1												
951	vs	951.3	vs	951.3	13_0^1	950	s	14_0^1									
967	m	967.5	m	966.2	39_0^2												
980	s	979.7	m	980.3	$21_0^1 25_0^2$												
984	m	984.8	vw	984.2	$14_0^1 25_0^2$												
1003	m	1003.4	m	1003	$14_0^1 25_0^1 48_0^2$												
		1036.4	m	1037	$13_0^1 25_2^3$												
1063	s	1062.9	m	1064	$15_0^2/13_0^1 25_1^2$												
1067	m	1067.5	m	1069	$14_0^1 23_0^1$												
1087	m	1086.8	m	1087	$20_0^1 25_0^1$												
1090	s	1090.7	m	1091	$13_0^1 25_0^1$												
		1110.1	w	1111	$13_0^1 48_0^2$												
1186	s	1185.7	w	1188	$13_0^1 47_0^2$												
1202	s	1202.4	w	1200	$14_0^1 16_0^1$												
		1226.8	m	1229	$13_0^1 25_0^2$	1228	m	$12_0^1 25_1^1$									
1253	vs	1253.1	s	1253	10_0^1	1251	s	12_0^1									
1268	m	1268.1	w		?												
1282	s	1280.8	m		?	1278	m	11_0^1									
1289	m				?												
1316	m	1315.8	vw	1314	$13_0^1 23_0^1$												
		1386.6	m	1386	$14_0^2 25_1^1$	1385	s	$18_0^2 25_1^1$									
1392	s	1392.6	vw	1393	$10_0^1 25_0^1$												

[a] Abbreviations: s, strong; m, medium; w, weak; v, very. [b] From ref 14. [c] Inferred combination frequencies are based on assignments of individual vibrations.

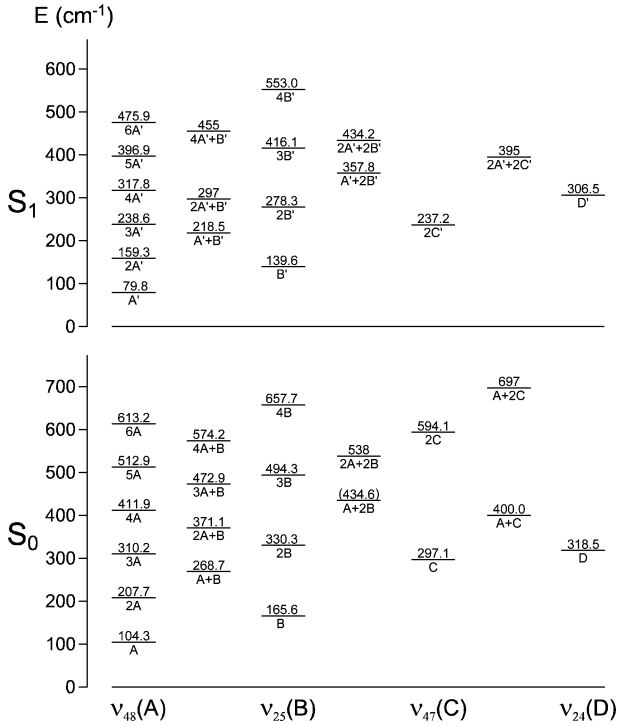

Figure 11. Energy level diagram for the low-frequency modes of 1,4-benzodioxan in its S_0 and $S_1(\pi,\pi^*)$ states.

assignments in the FES and UV absorption spectra. Assignments up to 2400 cm^{-1} higher than the 0_0^0 excitation are presented. The results from the earlier work of Gordon and Hollas[14] (GH) are also listed for comparison. The difference in assignments is obvious. The spectra in our work are much more comprehensive and thus have allowed a much clearer interpretation to be attained. For example, GH did not observe any bands in the 280−360 cm^{-1} region, but there are four bands evident in our FES and each band has a clear assignment. GH assigned the band at −138 cm^{-1} to be 24_1^1 and the band at 54 cm^{-1} to be 24_0^1, which would make the fundamental frequency of the double bond twisting vibration ν_{24} in the S_0 state be 192 cm^{-1}. This is not the case because the vapor-phase Raman spectrum[9] clearly shows the fundamental frequency of ν_{24} to be 317 cm^{-1}. Moreover, there is no band observed near 54 cm^{-1} in our work. The FES band at 306 cm^{-1} in our work is assigned to be 24_0^1, which is close to the computed frequency of 299 cm^{-1} from the CIS/6-311++G(d,p) basis set calculations for the S_1 excited state. Table 2 shows more than 130 assignments, almost all of which were made with considerable certainty. These were used to determine approximately 40 quantum states for both S_0 and S_1 states, and, therefore, the energy levels are each typically well-defined by several different spectroscopic transitions. It should be noted that a number of the observed transitions are not totally symmetric, and in principle these should be forbidden. However, as was the case for our work on phthalan, the highly anharmonic and larger amplitude vibrations often lead to violations of the first-order selection rules.

Figure 8 shows the single vibrational level fluorescence (SVLF) spectra collected from exciting the 0_0^0 band at 35 563.1 cm^{-1}. These frequencies and assignments are shown in Table 3. The fundamental frequencies obtained from vapor IR and vapor Raman spectra as well as those from B3LYP/6-311++G(d,p) calculations are also listed for comparison.[9] Figures 9 and 10 show the SVLF spectra from exciting the 25_0^1 and 48_0^2 bands, which are 139.2 and 158.6 cm^{-1} higher than the 0_0^0 band, respectively. The corresponding UV absorption spectra are also shown. The SVLF spectra were recorded from nine different excitation bands including 0_0^0. These corresponding results are summarized in Table 4. These data were very helpful in confirming the energies of the quantum levels for the S_0 ground state and also for determining the descriptions of the vibronic levels from which the transitions occur. Figure 11 presents the energy level diagram for both the S_0 and $S_1(\pi,\pi^*)$ states, based on all of these spectra. The four lowest-frequency ring vibrations ν_{48}, ν_{25}, ν_{47}, and ν_{24} are labeled as A, B, C, and D, respectively, and the corresponding quantum levels for the S_1 state are indicated by primes in both Table 4 and Figure 11. Table 5 compares the frequency assignments for several of the fundamental vibrations of 14BZD in its S_0 and $S_1(\pi,\pi^*)$ states.

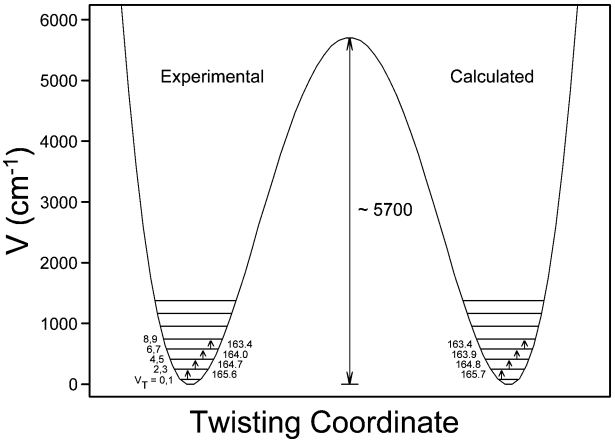

Figure 12. Experimental and calculated energy levels for the one-dimensional potential energy function of the ring-twisting vibration of 1,4-benzodioxan in its S_0 state.

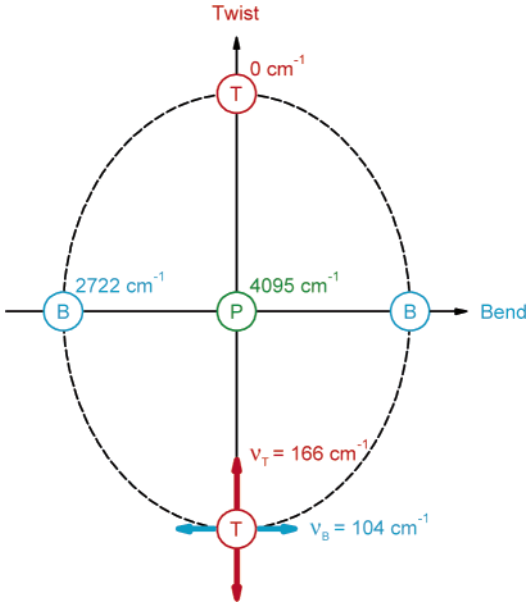

Figure 13. Representation of the two-dimensional potential energy for the ring-twisting and ring-bending vibrations of 1,4-benzodioxan in the S_0 state. P = planar; T = twisted; B = bent structure.

Potential Energy Surface (PES) for the S_0 Ground State

On the basis of the assignments of the low-frequency modes presented in Tables 3 and 4 and shown in Figure 11, both a one-dimensional potential energy function in terms of the ring-twisting vibration and a two-dimensional PES in terms of the

TABLE 3: Frequencies (cm^{-1}) and Assignments of Single Vibronic Level Fluorescence (SVLF) Spectra of Jet-Cooled 1,4-Benzodioxan with Excitation of the 0_0^0 Band at 35 563.1 cm^{-1} [a]

this work						from ref 9				
SVLF		UV		inferred[b]	assignment	vapor IR		vapor Raman		calcd[c]
0	vvs	0.0	vs	0	0_0^0					
−104	vw	−104.6	w		48_1^0			105	(8)	104
−166	s	−165.6	s		25_1^0			167	(15)	165
−207	vw			−208	48_2^0					
−297	vw	−297.1	w		47_1^0			297	(4)	297
−330	ms			−330	25_2^0					
−377	w				40_1^0					376
−400	m	−400.0	vw	−401	$47_1^0 48_1^0$					
−412	vw			−412	48_4^0					
−464	m	−464.0	vw	−463	$16_1^0/46_1^0/25_1^0 47_1^0$			463	(42)	462
−494	m			−494	$39_1^0/25_3^0$			495	(3)	494
−553	m	−552.2	vw		23_1^0			552	(11)	555
−562	s	−561.5	w		15_1^0	565	vw	566	(2)	571
−569	s	−568.4	m	−568	$46_1^0 48_1^0$					
−594	w	−594.1	m	−594	47_2^0					
−630	w			−630	$16_1^0 25_1^0/25_1^0 46_1^0$					
−643	w				38_1^0	645	vw			642
−659	w			−660/−658	$25_1^0 39_1^0/25_4^0$					
−697	vw			−698	$47_2^0 48_1^0$					
−717	m			−719	$22_1^0/23_1^0 25_1^0$					720
−727	m			−728	$15_1^0 25_1^0$					
−735	vs	−734.7	m	−735	$14_1^0/25_1^0 46_1^0 48_1^0$	733	vw	732	(100)	734
−747	m				45_1^0	746	s	746	(7)	747
−756	m	−755.5	vw	−754	40_2^0					
−843	m				21_1^0			842	vvw	845
−871	w			−871	$39_1^0 40_1^0$					
−881	w			−883	$22_1^0 25_1^0$					
−888	w			−890	47_3^0					
−893	m				13_1^0	893	ms	891	(1)	886
−901	s			−901	$14_1^0 25_1^0$					
−918	m				44_1^0					925
−953	w				20_1^0					952
−959	w			−958	$16_1^0 39_1^0/39_1^0 46_1^0$					
−1019	m			−1017	$16_1^0 23_1^0/23_1^0 46_1^0$					
−1028	s				12_1^0			1025	(65)	1029
−1043	m			−1044	$45_1^0 47_1^0$					
−1061	m			−1063	$36_1^0/39_1^0 46_1^0 48_1^0$					1059
−1067	m			−1067	$14_1^0 25_2^0$					
−1079	m				11_1^0	1074	s	1074	(1)	1066
−1105	m			−1106	$19_1^0/23_2^0$			1107	(4)	1105
−1122	m			−1124		15_2^0				
−1130	ms			−1131	$15_1^0 46_1^0 48_1^0$					
−1138	m			−1138	$46_2^0 48_2^0$					
−1150	w				10_1^0	1151	w	1151	(3)	1157
−1195	m			−1194	$34_1^0/12_1^0 25_1^0$	1194	w			1189
−1255	s				9_1^0	1250	s	1249	(25)	1252
−1268	m			−1271	$19_1^0 25_1^0$					
−1282	s				18_1^0	1280	s	1280	(29)	1286
−1289	s				33_1^0					1285
−1296	ms			−1297	$14_1^0 15_1^0$					
−1303	s			−1304	$8_1^0/14_1^0 46_1^0 48_1^0$	1307	ms	1306	(11)	1321
−1421	m			−1421	$9_1^0 25_1^0$					
−1433	m			−1434	22_2^0					
−1448	m			−1448	$18_1^0 25_1^0$					
−1469	s			−1470	$6_1^0/14_2^0$	1465	w	1462	(3)	1473

TABLE 3 (Continued)

this work				from ref 9				
SVLF	UV	inferred[b]	assignment	vapor IR		vapor Raman		calcd[c]
−1493	m	−1494	45_2^0					
−1500	m		5_1^0	1496	vs	1494	(0.5)	1502
−1588	m	−1590	$12_1^0 15_1^0$					
−1602	ms		4_1^0	1609	vw	1609	(4)	1602
−1628	m	−1628	$13_1^0 14_1^0$					
−1635	m	−1635	$6_1^0 25_1^0/14_2^0 25_1^0$					
−1649	m	−1648	$11_1^0 46_1^0 48_1^0$					
−1671	m	−1670	$20_1^0 22_1^0$					
−1686	m	−1686	21_2^0					
−1762	s	−1763	$12_1^0 14_1^0$					
−1815	m	−1814	$11_1^0 14_1^0$					
−1823	m	−1824	$9_1^0 46_1^0 48_1^0$					
−1837	m	−1836	44_2^0					
−1843	m	−1844	$15_1^0 18_1^0$					
−1849	s	−1851	$18_1^0 46_1^0 48_1^0/15_1^0 33_1^0$					
−1856	m	−1858	$33_1^0 46_1^0 48_1^0$					
−1919	w	−1918	$16_2^0 39_2^0 39_2^0 46_2^0$					
−1929	m	−1930	$14_1^0 34_1^0$					
−1989	s	−1990	$9_1^0 14_1^0$					
−2001	m	−2003	$44_2^0 25_1^0$					
−2014	s	−2017	$14_1^0 18_1^0$					
−2022	ms	−2014	$14_1^0 33_1^0$					

[a] Abbreviations: s, strong; m, medium; w, weak; v, very. [b] Inferred combination frequencies are based on assignments of individual vibrations. [c] Calculated using the B3LYP/6-311++G(d,p) basis set with GAUSSIAN 03.

TABLE 4: Single Vibronic Level Fluorescence (SVLF) Frequencies (cm^{-1}) and Assignments from Various Excitation Bands of 1,4-Benzodioxan[a]

excitation:		0_0^0	A′	B′	2A′	2C′	2B′	2A′ + B′	4A′	A′ + 2B′
assignment	inferred[b]	0[c] vs	+80 w	+139 s	+159 s	+237 s	+278 m	+297 m	+318 m	+358 m
A	−104.3	−104 vw	−104 s							
B	−165.6	−166 s		−166 vs	−166 m	−166 w	−165 s	−166 vw	−165 vw	
2A	−207.7	−207 vw		−208 vw	−208 vs	−207 vs		−207 ms	−207 m	
A + B	−268.7		−271 m	−270 vw						−270 vw
C	−297.1	−297 vw	−296 s		−295 vw					
2B	−330.3	−330 ms		−332 s	−330 w		−332 s	−332 m	−328 s	
2A + B	−371.1			−374 vw	−374 m	−374 m		−373 s		
40_1^0		−377 w								−377 vs
A + C	−400.0	−400 m		−401 vw	−400 s	−400 m		−400 s	−399 s	
4A	−411.9	−412 vw			−412 w					−411 vw
$16_1^0/46_1^0$	−462.7	−464 m		−465 vw					−464 w	−462 w
$3B/39_1^0$	−494.3	−494 m		−494 m	−494 w		−498 m	−496 w	−493 m	−493 vw
?				−499 m						
2A + 2B	−538							−539 ms		−540 m
23_1^0		−553 m		−553 w					−553 m	
15_1^0		−562 s		−566 m	−566 m	−567 w		−566 s	−566 ms	
$46_1^0 48_1^0$		−569 s								
2C	−594.1	−594 w			−594 m	−594 s		−594 m	−594 m	
$16_1^0 25_1^0/25_1^0 46_1^0$		−630 w		−631 w						
38_1^0		−643 w								
$4B/25_1^0 39_1^0$	−657.7	−659 w		−660 w			−659 w	−659 vw		
?			−665 m	−665 vw			−665 w			
A + 2C	−697	−697 vw	−698 w					−697 w		
$22_1^0/23_1^0 25_1^0$		−717 m		−717 w						
$15_1^0 25_1^0$		−727 m		−727 m						
$14_1^0/25_1^0 46_1^0 48_1^0$		−735 vs		−734 s	−735 w	−734 w	−733 w	−733 m		

[a] Abbreviations: s, strong; m, medium; w, weak; v, very. [b] Frequency values inferred from the energy level diagram in Figure 11. [c] The excitation of 0_0^0 is at 35 563.1 cm^{-1}; the frequencies of all other excitation bands are relative to the 0_0^0.

ring-twisting and ring-bending modes were calculated. Because the barrier to inversion through the twisting mode is very high and because the observed transitions only reach quantum states about 700 cm^{-1} above the energy minima, for both the one and two-dimensional calculations only the lower region of the PESs can be determined with considerable accuracy. Hence, the

TABLE 5: Comparison of Experimental Vibrational Frequencies (cm^{-1}) for 1,4-Benzodioxan in Its S_0 Ground and $S_1(\pi,\pi^*)$ Excited States

	ν				
sym. $C_{2v}(C_2)$	C_{2v}	C_2	description	S_0[a]	S_1[b]
A_1 (A)	10	12	C−H wag (op,op′)	1151	1253
	13	17	sat. ring (C−C) stretch	893	951
	14	19	benzene C−C stretch	735	706
	15	21	benzene ring bend	562	531
	16	23	sat. ring bend	463	493
A_2 (A)	20	16	C−H wag (op, op′)	953	947
	21	18	C−H wag (op, ip′)	843	702
	23	22	benzene ring bend	553	363
	24	24	skeletal twist	317	306
	25	25	sat. ring twist	166	140
B_1 (B)	37	41	benzene ring bend	834	889
	39	44	sat. ring bend	494	483
B_2 (B)	47	47	sat. ring flap	297	(119)[c]
	48	48	sat. ring bend	104	80

[a] Experimental frequencies are inferred from Table 4 and ref 9. [b] Experimental frequencies are inferred from Table 3. [c] Only overtone frequency of 237 cm^{-1} was observed for ν_{47}.

estimation of the barrier by extrapolation of the potential function in either case cannot be expected to be very accurate.

For the one-dimensional calculation, the potential energy-function is given by

$$V(\tau) = a\tau^4 + b\tau^2 \tag{2}$$

where τ is the ring-twisting coordinate, as defined in Figure 1. This calculation can be done in either reduced coordinates[15] or dimensioned coordinates, and the resulting calculated transition frequencies and barriers are the same in both cases. In reduced coordinates, the function that best fits the data is

$$V(\mathrm{cm}^{-1}) = 8.10(z^4 - 52.86z^2) \tag{3}$$

where z is the reduced coordinate. This function, which is shown in Figure 12, has a barrier to inversion of 5672 cm^{-1}, and the calculated frequencies agree well with the observed values, as shown in Table 6 and Figure 12. The coordinate z can be transformed to the dimensioned coordinate τ using[15]

$$\tau = (2\mu\mathrm{A})^{-1/2}\hbar z \tag{4}$$

where $\mu = 1/g_{44}$ is the reduced mass. The reduced mass that was calculated[12] for the simple twisting model is 30.0 au, but this large-amplitude vibration is clearly much more complicated than this model. If this reduced mass value is used, then the dimensioned potential function becomes

$$V(\mathrm{cm}^{-1}) = (1.68 \times 10^3)\tau^4 - (6.18 \times 10^3)\tau^2 \tag{5}$$

where τ is in radians. This function, however, has minima corresponding to ridiculously high twist angle values of ±77°. Part of the discrepancy is apparently related to the fact that the extrapolated barrier is 40% higher than the ab initio value of 4095 cm^{-1} and thus the minima are moved to higher τ values. The difficulty in having an accurate description of the vibrational model also contributes because a reliable reduced mass cannot be readily calculated. In addition to the twisting, the vibration no doubt also involves contributions from the out-of-plane and in-plane ring-bendings as well as CH_2 motions, particularly the rocking and twisting. To provide some perspective on the significance of the reduced mass, a reduced mass of $\mu = 100.0$ au

TABLE 6: Observed and Calculated One-Dimensional and Two-Dimensional Transition Frequencies (cm^{-1}) and the Corresponding Potential Energy Parameters for the 1,4-Benzodioxan S_0 Ground State

		one-dimensional[a]		two-dimensional[b]	
parameters	observed	calcd I	calcd II	calcd III	calcd IV
μ_{twist}		30.0	100.0	29.9	84.3
a (cm^{-1}/rad^4)		1.68×10^3	1.87×10^4	6.4×10^3	3.7×10^4
b (cm^{-1}/rad^2)		-6.18×10^3	-2.06×10^4	-1.0×10^4	-2.8×10^4
c (cm^{-1}/rad^2)				2.8×10^3	2.8×10^3
d (cm^{-1}/rad^4)				1.0×10^3	2.3×10^3
A		8.10	8.10	12.68	11.43
B		−52.86	−52.86	−35.10	−43.23
barriers (cm^{-1})		5672	5672	3906	5339
τ_{min} (rad)		1.35	0.74	0.88	0.61
τ_{min} (degree)		77°	42°	50°	35°
(0,0)−(2,0)	165.6	165.7	165.7	166.7	166.0
(2,0)−(4,0)	164.7	164.8	164.8	164.8	164.6
(4,0)−(6,0)	164.0	163.9	163.9	163.2	163.4
(6,0)−(8,0)	163.4	163.4	163.4	162.4	163.1
(0,1)−(2,1)	164.4			166.6	165.6
(0,2)−(2,2)	163.4			166.6	165.2
(0,0)−(0,1)	104.3			104.1	104.3
(0,1)−(0,2)	103.4			103.9	104.2
(0,2)−(0,3)	102.5			103.8	104.1
(0,3)−(0,4)	101.7			103.7	104.0
(0,4)−(0,5)	101.0			103.5	103.8
(0,5)−(0,6)	100.3			103.4	103.7
(0,6)−(0,7)	99.8			103.2	103.6
(2,0)−(2,1)	103.1			104.0	103.9
(2,1)−(2,2)	102.4			103.9	103.8
(2,2)−(2,3)	101.8			103.8	103.6
(2,3)−(2,4)	101.3			103.6	103.5
(4,0)−(4,1)	102.8			104.0	103.5
(4,1)−(4,2)	102.0			103.9	103.4

[a] The one-dimensional potential function is given by $V = a\tau^4 + b\tau^2$. [b] The two-dimensional potential function is given by $V = a\tau^4 + b\tau^2 + c\theta^2 + d\tau^2\theta^2$.

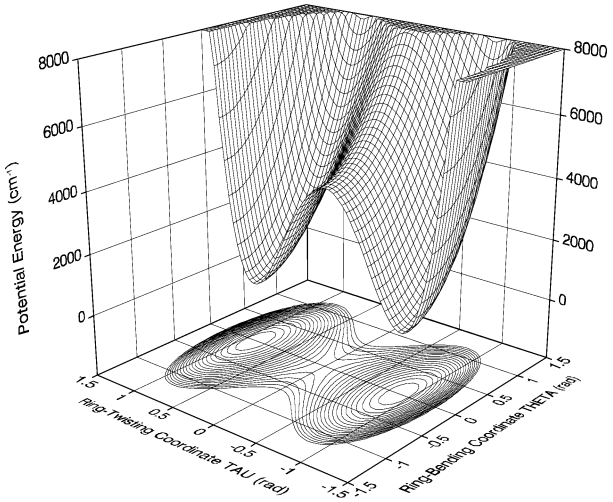

Figure 14. Two-dimensional potential energy surface for the ring-twisting coordinate τ and the ring-bending coordinate θ of 1,4-benzodioxan in its S_0 state.

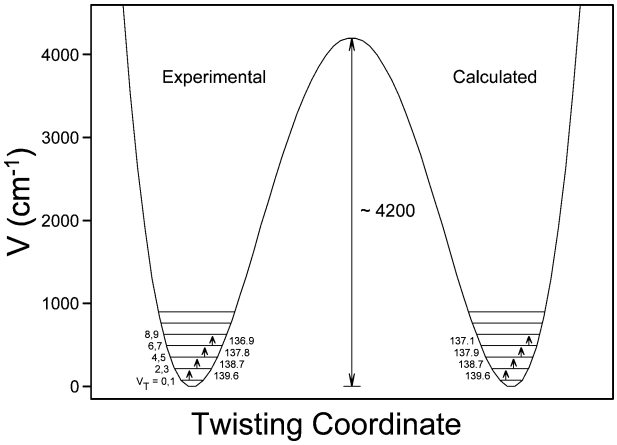

Figure 15. Experimental and calculated energy levels for the one-dimensional potential energy function of the ring-twisting vibration of 1,4-benzodioxan in its S_1 state.

was arbitrarily utilized to recalculate the dimensioned potential function and this was found to be

$$V(\mathrm{cm}^{-1}) = (1.87 \times 10^4)\tau^4 - (2.06 \times 10^4)\tau^2 \qquad (6)$$

For this function, the twisting angles are $\pm 42°$, which are much closer to the ab initio values of $\pm 30°$.

The experimental data in this case, therefore, do not do a particularly good job of determining the barrier because they only show the barrier to be very high. The experimental results can be stated to be 5000 ± 2000 cm^{-1} for the one-dimensional model. Prediction of the twisting angle is even worse. Again only the fact that there is a large twist angle can be ascertained.

To account for some of the vibrational coupling involving the ring-twisting mode, a two-dimensional calculation with the out-of-plane ring-bending coordinate added, was also carried out. Figure 13 presents a graphical view, based on the ab initio calculations, of the relative energies of the twisted (T), bent (B), and planar (P) conformations. The molecule is trapped in its twisted structure where the twisting frequency is 166 cm^{-1} and the bending frequency is 104 cm^{-1}. The molecule can undergo hindered pseudorotation and pass over a saddle point at 2722 cm^{-1} corresponding to a bent configuration. This is a lower energy pathway than that ascending over the planar structure at 4095 cm^{-1}. Although the bent form is considerably lower in energy than the planar form, the data for the bending vibration, which extend to about 700 cm^{-1} above the ground state, are also not sufficient to yield a reliable experimental

TABLE 7: Observed and Calculated One-Dimensional and Two-Dimensional Transition Frequencies (cm^{-1}) and the Corresponding Potential Energy Parameters for the 1,4-Benzodioxan $S_1(\pi,\pi^*)$ Excited State

		one-dimensional[a]		two-dimensional[b]	
parameters	observed	calcd I	calcd II	calcd III	calcd IV
μ_{twist}		28.5	100.0	28.3	72.0
a (cm^{-1}/rad^4)		1.04×10^3	1.29×10^4	4.4×10^3	2.6×10^4
b (cm^{-1}/rad^2)		-4.17×10^3	-1.46×10^4	-5.5×10^3	-1.3×10^4
c (cm^{-1}/rad^2)				2.1×10^2	4.9×10^2
d (cm^{-1}/rad^4)				3.2×10^3	7.1×10^3
A		7.15	7.15	11.61	11.61
B		−48.22	−48.22	−24.51	−24.51
barriers (cm^{-1})		4158	4158	1744	1672
τ_{min} (rad)		1.41	0.75	0.79	0.50
τ_{min} (degree)		81°	43°	45°	29°
(0,0)−(2,0)	139.6	139.6	139.6	139.5	140.3
(2,0)−(4,0)	138.7	138.7	138.7	138.9	138.7
(4,0)−(6,0)	137.8	137.9	137.9	137.8	137.2
(6,0)−(8,0)	136.9	137.1	137.1	136.9	136.4
(0,1)−(2,1)	138.7			138.4	139.2
(0,2)−(2,2)	137.7			137.3	138.0
(0,0)−(0,1)	79.8			80.3	80.5
(0,1)−(0,2)	79.5			79.9	79.9
(0,2)−(0,3)	79.3			79.4	79.4
(0,3)−(0,4)	79.2			79.0	78.9
(0,4)−(0,5)	79.1			78.6	78.4
(0,5)−(0,6)	79.0			78.2	78.0
(2,0)−(2,1)	78.9			79.2	79.3
(2,1)−(2,2)	78.5			78.7	78.8
(4,0)−(4,1)	79.5			77.7	78.0
(4,1)−(4,2)	76.4			77.3	77.5

[a] The one-dimensional potential function is given by $V = a\tau^4 + b\tau^2$. [b] The two-dimensional potential function is given by $V = a\tau^4 + b\tau^2 + c\theta^2 + d\tau^2\theta^2$.

energy value for the bent structure. Therefore, the following two-dimensional form of the PES was utilized

$$V(\tau, \theta) = a\tau^4 + b\tau^2 + c\theta^2 + d\tau^2\theta^2 \qquad (7)$$

where τ and θ are the ring-twisting and ring-bending coordinates defined in Figure 1. For this PES the *a* and *b* coefficients define the twisting energetics. The parameter *c* is the coefficient for the harmonic term for the bending because this motion is very nearly harmonic in the region of the twisting minima (T). The data do not allow for a determination of the energy of the bent saddle points (B). Finally, the parameter *d* represents the interaction between the two modes. The two modes also interact through the g_{45} kinetic energy cross term discussed earlier. The parameters that best fit the data are $a = 6.4 \times 10^3$ cm^{-1}/rad^4, $b = -1.0 \times 10^4$ cm^{-1}/rad^2, $c = 2.8 \times 10^3$ cm^{-1}/rad^2, and $d = 1.0 \times 10^3$ cm^{-1}/rad^4, and these correspond to a twisting barrier of 3906 cm^{-1}, which is much closer to the ab initio value of 4095 cm^{-1}. Here again, however, the energy minima depend on the reduced mass values. The computed two-dimensional value of 29.9 au for the twisting produces minima at $\pm 50°$. A value of 84.3 au would be required to match the ab initio value of $\pm 30°$.

The calculated frequencies for the two-dimensional PES are shown in Table 6, and Figure 14 shows this surface. The frequency agreement is excellent because it does not depend on the reduced mass values. Because no quadratic term was used in the potential energy function for the bending angle θ, this surface cannot show the presence of a saddle point along the bending axis although it is almost certainly present.

Potential Energy Surface for the $S_1(\pi,\pi^*)$ Excited State

Similar procedures were carried out for studying the $S_1(\pi,\pi^*)$ excited state, and the data in Table 2 and Figure 11 were used. The one-dimensional potential energy function for the ring-twisting vibration in reduced coordinate is

$$V(\text{cm}^{-1}) = 7.15(z^4 - 48.22z^2) \qquad (8)$$

This function has a barrier of 4158 cm^{-1} and is shown in Figure 15. Table 7 shows the agreement between observed and calculated transition frequencies, and this is nearly perfect.

If the calculated reduced mass of 28.5 au is used to transfer to the dimensioned coordinate τ, then the potential energy function becomes

$$V(\text{cm}^{-1}) = (1.04 \times 10^3)\tau^4 - (4.17 \times 10^3)\tau^2 \qquad (9)$$

and this function has minima at $\pm 81°$, which again is ridiculously high. As shown in Table 7, the arbitrary reduced mass of 100.0 au would produce twisting angles of $\pm 43°$.

A two-dimensional calculation based on eq 7 was also carried out, and the parameters determined are $a = 4.4 \times 10^3$ cm^{-1}/rad^4, $b = -5.5 \times 10^3$ cm^{-1}/rad^2, $c = 2.1 \times 10^2$ cm^{-1}/rad^2, and $d = 3.2 \times 10^3$ cm^{-1}/rad^4. For this case, the calculated barrier is 1744 cm^{-1} and the energy minima are at $\pm 45°$. The limited experimental data along with the inaccuracy of ab initio calculations for the excited state, however, do not give much confidence in these results. Because the twisting frequencies decrease from the 166 cm^{-1} in the S_0 ground state to 140 cm^{-1} in the S_1 excited state, this does indicate that the excited-state barrier is lower. Moreover, the one-dimensional potential energy calculations, based on our experimental data which yield a drop of 5672 cm^{-1} to 4158 cm^{-1}, strongly support this view. An educated guesstimate is that the S_1 excited-state barrier is about 3600 ± 2000 cm^{-1} versus 5000 ± 2000 cm^{-1} for the S_0 ground state.

Acknowledgment. We thank the National Science Foundation (Grant CHE-0131935) and the Robert A. Welch Foundation (Grant A-0396) for financial assistance. We also thank Dr. Jaebum Choo for performing some complementary calculations.

References and Notes

(1) Laane, J. *J. Phys. Chem. A* **2000**, *104*, 7715.
(2) Laane, J. *Intl. Rev. Phys. Chem.* **1999**, *18*, 301.
(3) Sakurai, S.; Bondoc, E.; Laane, J.; Morris, K.; Meinander, N.; Choo, J. *J. Am. Chem. Soc.* **2000**, *122*, 2628.
(4) Bondoc, E.; Sakurai, S.; Morris, K.; Chiang, W.-Y.; Laane, J. *J. Chem. Phys.* **2000**, *112*, 6700.
(5) Arp, Z.; Meinander, N.; Choo, J.; Laane, J. *J. Chem. Phys.* **2002**, *116*, 6648.
(6) Yang, J.; Wagner, M.; Okuyama, K.; Morris, K.; Arp, Z.; Choo, J.; Meinander, N.; Laane, J. *J. Chem. Phys.*, submitted for publication, 2006.
(7) Arp, Z.; Laane, J.; Sakamoto, A.; Tasumi, M. *J. Phys. Chem.* **2002**, *106*, 3479.
(8) Autrey, D.; Arp, Z.; Choo, J.; Laane, J. *J. Chem. Phys.* **2003**, *119*, 2557.
(9) Autrey, D.; Yang, J.; Laane, J. *J. Mol. Struct.* **2003**, *661*, 23.
(10) Frisch, M. J.; Trucks, G. W.; Schlegel, H. B.; Scuseria, G. E.; Robb, M. A.; Cheeseman, J. R.; Montgomery, J. A., Jr.; Vreven, T.; Kudin, K. N.; Burant, J. C.; Millam, J. M.; Iyengar, S. S.; Tomasi, J.; Barone, V.; Mennucci, B.; Cossi, M.; Scalmani, G.; Rega, N.; Petersson, G. A.; Nakatsuji, H.; Hada, M.; Ehara, M.; Toyota, K.; Fukuda, R.; Hasegawa, J.; Ishida, M.; Nakajima, T.; Honda, Y.; Kitao, O.; Nakai, H.; Klene, M.; Li, X.; Knox, J. E.; Hratchian, H. P.; Cross, J. B.; Bakken, V.; Adamo, C.; Jaramillo, J.; Gomperts, R.; Stratmann, R. E.; Yazyev, O.; Austin, A. J.; Cammi, R.; Pomelli, C.; Ochterski, J. W.; Ayala, P. Y.; Morokuma, K.; Voth, G. A.; Salvador, P.; Dannenberg, J. J.; Zakrzewski, V. G.; Dapprich, S.; Daniels, A. D.; Strain, M. C.; Farkas, O.; Malick, D. K.; Rabuck, A. D.; Raghavachari, K.; Foresman, J. B.; Ortiz, J. V.; Cui, Q.; Baboul, A. G.; Clifford, S.; Cioslowski, J.; Stefanov, B. B.; Liu, G.; Liashenko, A.; Piskorz, P.; Komaromi, I.; Martin, R. L.; Fox, D. J.; Keith, T.; Al-Laham, M. A.; Peng, C. Y.; Nanayakkara, A.; Challacombe, M.; Gill, P. M. W.; Johnson, B.; Chen, W.; Wong, M. W.; Gonzalez, C.; Pople, J. A. *Gaussian 03*, revision C.02; Gaussian, Inc.: Wallingford, CT, 2004.
(11) Yang, J. Ph.D. Dissertation, Texas A&M University, 2006.
(12) Yang, J.; Laane, J. *J. Mol. Struct.*, in press, 2006.
(13) Tecklenburg, M. M. J.; Laane, J. *J. Am. Chem. Soc.* **1989**, *111*, 6920.
(14) Gordon, R. D.; Hollas, J. M. *J. Mol. Spectrosc.* **1994**, *163*, 159.
(15) Laane, J. *Appl. Spectrosc.* **1970**, *24*, 73.